Xiong et al. *NPG Asia Materials* (2022) 14:84
https://doi.org/10.1038/s41427-022-00431-2

NPG Asia Materials

ARTICLE Open Access

High-speed magnetic control of water transport in superhydrophobic tubular actuators

Fangyihan Xiong[1], Liyun Zhang[1], Lei Xu[1], Huan Zhao[1], Jianyang Lan[1], Chenhao Ji[1], Linfeng Chen[1,2] and Fan Xia[1,2,3]

Abstract

Directed transport of a small amount of water is a basic issue and has attracted extensive attention due to its importance in a wide range of applications, such as water collection, microfluidics, printing, bioanalysis, and microchemical reactions. Various strategies based on constructing a surface tension gradient or Laplace pressure gradient have been developed to realize directional water transport. Typically, electrostatic forces and magnetic fields are utilized to achieve high-speed water transport on open superhydrophobic surfaces. However, these methods suffer from water evaporation or contamination. Here, we report a magnetic superhydrophobic tubular PDMS actuator for directional water transport. The actuator deformed under an applied external magnetic field and actuated the water droplet to transport along the moving direction of the magnet. The water transport velocity reached 16.1 cm/s. In addition, as the inner surface of the actuator is superhydrophobic, the water droplet showed weak interactions with the surface and presented negligible mass loss during the transport process. The results of this work may inspire new design of actuators for directional water transport with high speeds.

Introduction

Water-based liquid manipulation has attracted considerable attention in recent decades due to its fundamental importance in a broad range of applications, such as water collection[1–3], microfluidics[4–6], condensation and heat transfer[7–9], self-cleaning[10], printing[11,12], bioanalysis[13–15], oil/water separation[16–18], and microchemical reactions[19,20]. Nature provides excellent examples of directional water transport. For example, beetles in the Namib Desert can collect water from the air by using unique hydrophilic-hydrophobic patterns on their backs to survive in the desert[21]. By repeatedly opening and closing their beaks, shorebirds can control the capillary force that transports water droplets mouthward[22]. A cactus featuring conical spines utilizes the asymmetric structure-induced force to efficiently capture fog and move the water droplets from the tip to the base[23].

Various nature-inspired strategies have been successfully developed for self-propelled water transport either by constructing chemical gradients on substrates or by fabricating asymmetric structures[17,24–27]. However, these passive methods generally suffer from quite low water transport velocities or short transport distances[28,29], which limit practical application. In recent years, the peristome surface of the pitcher plant has provided inspiration for fabricating materials that present high water transport velocities over relatively long distances[30,31]. However, this requires the substrate to be superhydrophilic, which inevitably causes significant liquid loss during the transport process. In addition, it is still a technical challenge to easily fabricate the complex structure of the peristome surface of the pitcher plant. Alternatively, active strategies, such as magnetic fields[20,32,33], electrostatic forces[34,35], and heat[36–38], have also been utilized to direct water transport with high speeds on open surfaces. For example, magnetic actuation has attracted particular interest due to its susceptibility to

Correspondence: Linfeng Chen (chenlinfeng@cug.edu.cn)
[1]Faculty of Materials Science and Chemistry, China University of Geosciences, Wuhan 430074, People's Republic of China
[2]State Key Laboratory of Biogeology and Environmental Geology, China University of Geosciences, Wuhan 430074, People's Republic of China
Full list of author information is available at the end of the article
These authors contributed equally: Fangyihan Xiong, Liyun Zhang

remote control and easy operation. By coating magnetic nanoparticles on the droplet surface or by adding magnetic materials into the droplet, water droplets on superhydrophobic surfaces can be actuated with magnetic fields[39–41]. However, these strategies inevitably lead to contamination, loss of magnetic response due to detachment of the magnetic materials from the liquid droplets, and significant liquid loss due to evaporation. Recently, interesting tubular actuators have been reported for directional liquid transport[42,43], but the water transport velocity is quite low due to the large wetting hysteresis.

Here, we propose a magnetic superhydrophobic polydimethylsiloxane (PDMS) tubular actuator (M-SPDMS-A) for use in directional water transport. The actuator is composed of a PDMS tube with one side of the tube outer surface coated with magnetic nanoparticles. The inner surface of the actuator is rough and superhydrophobic. Upon applying an external magnetic field with a predefined direction of motion, the actuator deforms correspondingly and actuates the water droplet inside the tube to move forward (Fig. 1a). As the inner surface of the actuator is superhydrophobic, the droplet is easily driven to move with speeds reaching up to 16.1 cm/s. In addition, the water droplet presents negligible liquid loss due to the superhydrophobic property of the actuator. In Fig. 1b, an M-SPDMS-A is shown to actuate a water droplet inside the tube from left to right under the control of an external magnetic field (Movie S1).

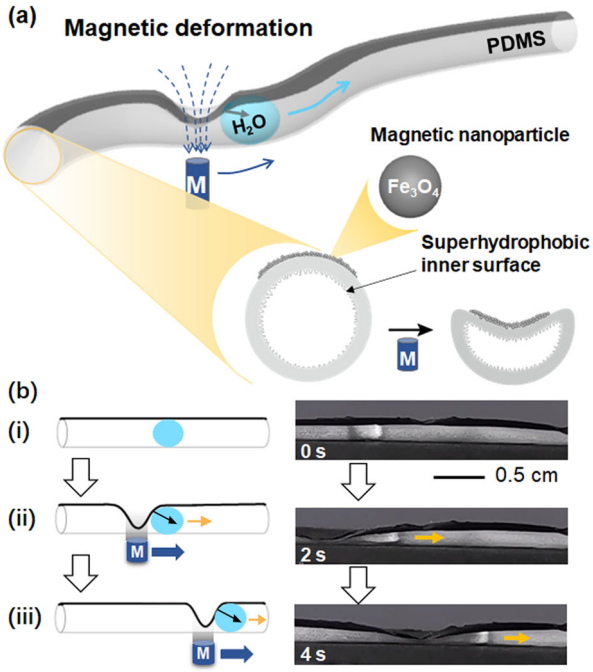

Fig. 1 Design of the magnetic superhydrophobic PDMS tubular actuator (M-SPDMS-A). a Schematic illustration of the structure of M-SPDMS-A and magnetic transport of a water droplet. The M-SPDMS-A deforms in response to an applied magnetic field. As the inner surface of the actuator is superhydrophobic, water droplets can be easily transported along the moving direction of the magnet. **b** Magnetic field-induced water droplet transport in the M-SPDMS-A. The left panel shows a schematic of the magnetic field-induced deformation of M-SPDMS-A and water droplet transport. The right panel shows the corresponding experimental results for magnetic control of water transport from left to right (Movie S1).

Materials and methods

Materials

Industrial Al (99+%, Mingxi Bonsai Modeling Tools, Jiangsu, China) rods (1, 2, and 3 mm in diameter) were cut to lengths of approximately 11 cm and used as templates for tubular PDMS preparation. Hydrochloric acid (HCl), sodium hydroxide (NaOH), and nitric acid (HNO_3) were purchased from Innochem (China). Ethanol and rhodamine B (RhB) were purchased from Hushi (Shanghai, China). PDMS (Sylgard184, monomer and curing agent) was purchased from Dow Corning. Iron oxide (Fe_3O_4) nanoparticles were purchased from Aladdin. Artificial urine (pH 4.5) and artificial sweat (pH 5.5) were purchased from ChuangFeng Technology (Dongguan, China). Phosphate buffer solution (PBS, 0.1 M, pH 7.4) was purchased from Sigma. The cylindrical magnets used were 5 mm in diameter and 2 cm in length. Unless otherwise specified, all magnetic control experiments were performed with a magnetic field intensity of approximately 306 mT.

Instruments

Scanning electron microscopy (SEM) images and energy-dispersive X-ray spectroscopy (EDS) images were collected with a field-emission scanning electron microscope (SU8010, HITACHI, Japan) equipped with EDS (BRUKER AXS, Germany). PDMS samples were coated with a thin layer of gold prior to SEM examination, which was performed on a magnetron ion sputter metal coating device (MSP-2S, Japan). The sliding angles (SA) and contact angles (CA) of the inner surfaces of PDMS actuators were measured with a contact angle goniometer (DSA100). Fourier transform infrared spectroscopy (FTIR) was performed with a ThermoFisher Nicolet iS5. The fluorescence of RhB left on the PDMS actuators was measured with a laser scanning confocal microscopy (LSM880 confocal microscopy, Carl Zeiss AG) equipped with a FemtoSecond Laser (Coherent Inc.). The transport process of water droplets in the PDMS tubular actuator was recorded with a mobile telephone camera.

Fabrication of Al molds and tubular PDMS

Al molds were fabricated according to a previously reported method[44]. Al rods were first immersed in NaOH solution (0.5 M) for 5 min to remove the oxide layer.

Then, the Al rods were etched to produce microstructures by immersing the rods in HCl solution (2.5 M) for 30 min, followed by washing with ultrapure water. Subsequently, the structured Al rods were placed in a mixture of HNO_3 and water (volume ratio 1:4) and treated by ultrasonication for 5 min to remove residual ions. The as-obtained Al rods were then placed in boiling deionized water for 30 min to obtain nanostructures. Finally, the Al molds were completely washed with ultrapure water and dried for the preparation of PDMS tubes.

A mixture of PDMS monomer and curing agent in a 10:1 wt. ratio was first degassed under vacuum for 20 min. Then, Al molds were vertically inserted into the degassed PDMS prepolymer, followed by vacuum pumping for 120 min to completely remove the air between the structured surfaces of the molds and the liquid PDMS. Al rods coated with PDMS prepolymer were vertically positioned for a certain amount of time (5, 10, 20, 30, and 60 min) at room temperature to tune the thickness of the PDMS coating, followed by curing in an oven at 90 °C for 3 h. PDMS tubes with different thicknesses were finally obtained by sequentially removing the Al templates with acid etching and washing completely with ultrapure water. PDMS tubes without inner structures were also prepared as controls with procedures similar to those described above, except that Al rods without acid etching were used as templates. Unless otherwise specified, all other experiments were completed at room temperature.

Preparation of magnetic PDMS tubular actuators

Iron oxide (Fe_3O_4) nanoparticles (60 wt%) were first homogeneously mixed with PDMS prepolymer (monomer to initiator weight ratio 10:1). Then, the mixture was coated onto a clean plastic plate by the blade coating process. The thickness was controlled by using a piece of cover slide (~0.13 mm in thickness) as a spacer. The plastic plate was fixed with the magnetic particle-doped polymer film facing down. As-prepared PDMS tubes were then fixed on a lab jack and brought into contact with the magnetic PDMS prepolymer for coating. Subsequently, the PDMS tubes coated with the magnetic layer were placed in an oven for curing at 50 °C for 4 h to finally give the magnetic PDMS tubular actuators (Fig. S1).

Magnetic control of liquid transport in a magnetic PDMS tubular actuator

The magnetic superhydrophobic PDMS tubular actuator (M-SPDMS-A) was fixed with doubly adhesive tape on a piece of black paper (~0.22 mm in thickness). The black paper was relatively hard and supported the actuator. A cylinder magnet (5 mm in diameter, 2 cm in length, and with a surface magnetic intensity of approximately 306 mT) was placed at the bottom of the paper and moved back and forth along the longitudinal direction of the actuator with manually controlled moving velocities. A liquid droplet (~10–25 μL, including water, PBS, artificial urine, and artificial sweat) was added into the actuator with a pipette. Then, the magnet was manipulated to move horizontally from one side of the actuator to the other side, propelling the liquid to transport directionally. The magnetic water transport process was recorded with a mobile telephone camera and analyzed later.

Magnetic control of water transport along a slope or an arch-shaped substrate was performed similarly to those described above except that the paper supporter was placed to form a slope with a certain tilt angle or an arch-shaped substrate. Coalescence of two water droplets controlled by the magnetic field was completed by first adding two water droplets (to distinguish the two water droplets, RhB was selectively added to one of them) sequentially into the actuator and then propelling one of the droplets to move with the magnetic field and coalesce with the other droplet. A solid resin sphere was carried and conveyed by placing the millimeter sphere inside the tubular actuator and then applying the magnetic field to drive the water droplet to move toward the sphere.

Water transport driven by gravity was carried out by placing the M-SPDMS-A on constructed slopes with different tilted angles (5°, 8°, 15°, and 19°). Then, a water droplet was added with a pipette into the actuator. The water motion down the slopes was then recorded.

Liquid loss test of water transport in magnetic tubular actuators

A liquid droplet (e.g., water, PBS, artificial urine, and artificial sweat) (~10 μL) with a RhB concentration of 10^{-6} M was added into the M-SPDMS-A fixed on a piece of paper (~0.22 mm in thickness). Then, the cylindrical magnet was manipulated to move horizontally along the longitudinal direction of the actuator at a speed of ~3 mm/s. The water transport process was recorded by a mobile telephone camera. The inner surface of the sample was collected and characterized by LSM880 confocal microscopy. To confirm whether the inner surface of the M-SPDMS-A exhibited a fluorescence signal, a control sample of the M-SPDMS-A that was not used for liquid transport was prepared for confocal microscopy.

A magnetic hydrophobic PDMS tubular actuator (i.e., there was no microstructure on the inner surface) was also prepared as a control for the liquid loss experiment. The liquid transport procedure was similar to that of the M-SPDMS-A. As the liquid droplet could not be propelled to move, the inner surface was used for confocal microscopy after the liquid was removed by tissue paper.

The samples used for water transport were all characterized by SEM to observe any microscale changes.

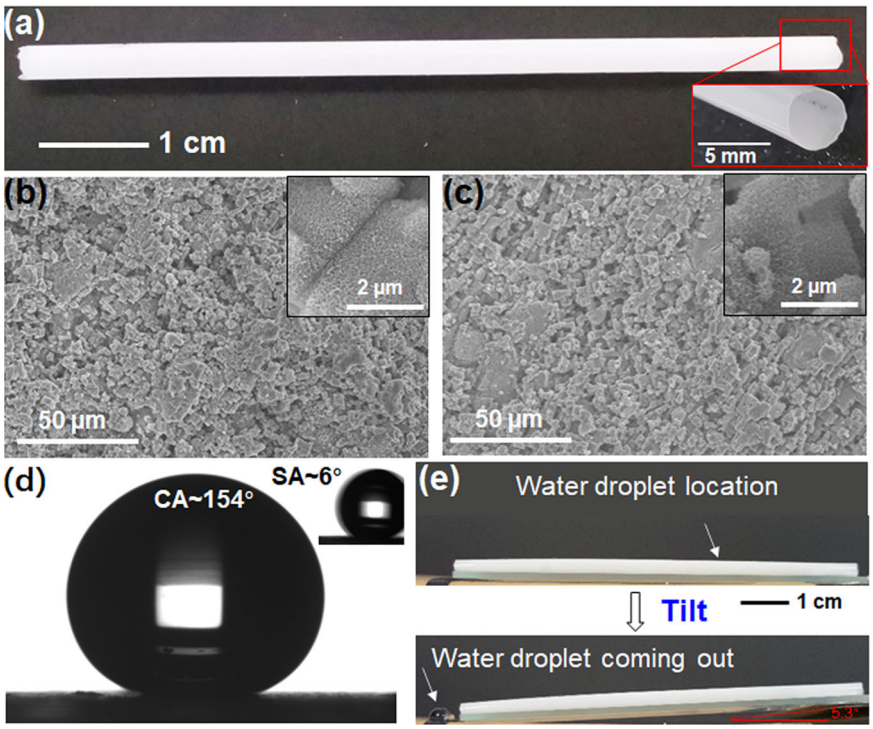

Fig. 2 Structure and superhydrophobicity for Al rod template-assisted preparation of PDMS tube. a Lateral photograph of a PDMS tube with a diameter of 3 mm. The inset is a cross-sectional view of the tube. **b** SEM image of the inner surface of (**a**). **c** SEM image of the Al rod template. **d** Contact angle and slide angle of the inner surface of the PDMS tube. **e** Water droplet is removed easily from the PDMS tube when the tube is tilted with an angle of approximately 5.3°, since the inner surface of the PDMS tube is superhydrophobic.

Results and discussion

Superhydrophobic tubular PDMS was prepared with a modified method[44]. Unless otherwise specified, the properties of the superhydrophobic PDMS we demonstrate in detail in the following section are for samples with an inner diameter of 3 mm. An as-prepared tubular PDMS sample with a length of approximately 7.5 cm is shown in Fig. 2a. It was white in appearance (Fig. 2a) due to the presence of the microstructure. In comparison, the tubular PDMS obtained from the Al rod template without treatment was relatively transparent (Fig. S2). SEM characterization confirmed that the inner surfaces of the PDMS had micro/nano hierarchical structures (Fig. 2b) that were similar to that of the Al rod template (Fig. 2c), indicating good replication of the structure from the Al rod. Energy dispersive X-ray spectroscopy (EDS) and Fourier transform infrared spectroscopy (FTIR) showed that the inner surface of the obtained PDMS tube was clean and without contamination (Figs. S3, S4). It is well known that rough surfaces combined with low surface tension chemicals are usually superhydrophobic[45,46]. For instance, glass substrates coated with SiO_2 nanoparticles and modified with fluorinated molecules (e.g., 1H, 1H, 2H, 2H-perfluorooctyltrichlorosilane) present contact angles >150°[29]. The surface tension of PDMS is approximately 20 mN/m; thus, the inner surface of the PDMS tube is expected to be superhydrophobic. A piece of PDMS was cut for testing. As shown in Fig. 2d, the contact angle (CA) and slide angle (SA) of the inner surface of the PDMS tube were measured to be ~154° and ~6°, respectively. Without a micro/nanostructure, the PDMS was hydrophobic with a CA ~110° (Fig. S2b, c). For the superhydrophobic sample, adhesion of the water droplet on the inner surface was low, and the water droplet moved easily along the tilted tube (~5.3°) under gravity (Fig. 2e). The method is applicable for preparing superhydrophobic PDMS tubes with different diameters. Superhydrophobic PDMS samples with inner diameters of 1 mm and 2 mm are shown in Fig. S5.

The superhydrophobic tubular PDMS was further coated with magnetic nanoparticles on its outer surface by using a contact coating method, as briefly shown in Fig. S1. Typically, a film of PDMS prepolymer containing iron oxide nanoparticles (60 wt.%) (Fig. S7) was prepared on a piece of plastic plate and placed with the magnetic film side facing down. Then, the PDMS tube fixed on a lab jack was brought into contact with the magnetic film for coating, followed by heat curing. As shown in Fig. 3a, magnetic PDMS was obtained. A black thin magnetic layer was clearly observed to coat one side of the PDMS

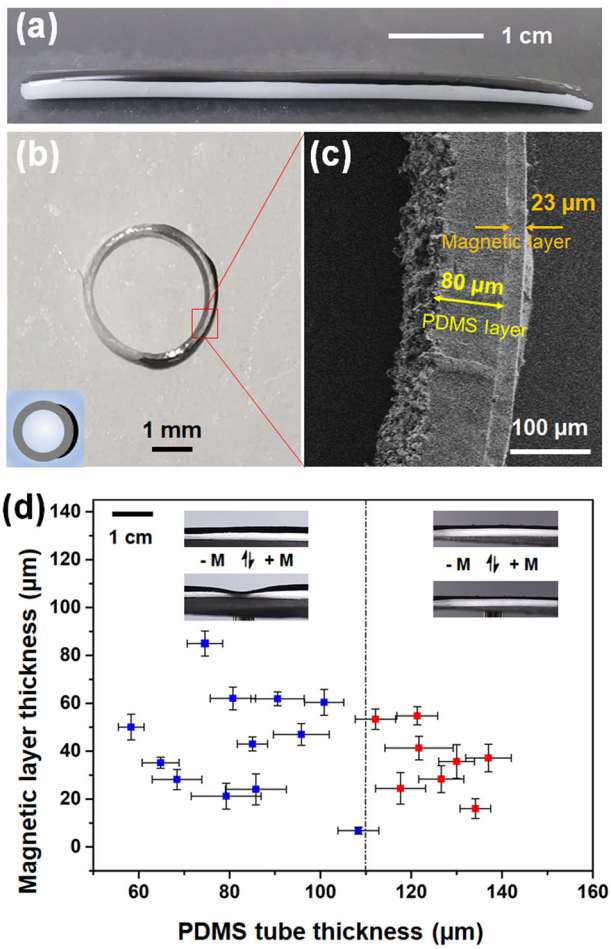

Fig. 3 Characterization and properties of the M-SPDMS-A. **a** Lateral image of the M-SPDMS-A. The black coating is the magnetic layer. **b** Cross-sectional image of the M-SPDMS-A. The inset cartoon shows the orientation of the magnetic coating. **c** SEM image of the cross section of the sample in (**b**). The width of the magnetic layer is ca. 23 μm, and that of the inner PDMS layer is ca. 80 μm. **d** Magnetic deformation of the M-SPDMS-A versus the thickness of the magnetic coating (*y*) and the inner PDMS layer (*x*), as indicated in (**c**). It is difficult to deform the M-SPDMS-A magnetically when *y* is larger than 110 μm (the right part), while it can be deformed when *y* is less than 110 μm (the left part). The inset shows photographs of M-SPDMS-A responding to a magnetic field in different cases.

outer surface from the lateral and cross-section views (Fig. 3a, b). SEM showed that the thickness of the PDMS tube (denoted as *x*) and the magnetic layer (denoted as *y*) were ~80 and ~23 μm, respectively (Fig. 3c). The thicknesses of the PDMS and the magnetic layers could be tailored on demand. After coating with PDMS prepolymer, the Al rod templates were aligned vertically. By tuning the time (*t*), PDMS tubes with different thicknesses (*x*) were obtained (Fig. S7). The thickness was ~141 μm when *t* was ~5 min. The thickness decreased to ~71 μm when *t* was extended up to 20 min, and a small change in *x* occurred with increasing time. The thickness of the magnetic layer (*y*) could be controlled by changing the thickness of the magnetic prepolymer film on the plastic plate.

Magnetic deformation of the PDMS is a prerequisite to realizing directional water transport, which involves controlling the proper thickness of the PDMS tube and the magnetic layer. The magnetic properties of Fe_3O_4 nanoparticle-coated PDMS tubes were studied. We fixed the magnetic tubular PDMS on a piece of paper (thickness approximately 0.22 mm) with the magnetic layer facing up. The paper was relatively stiff and supported the PDMS actuator. Then, we used a cylindrical magnet (5 mm in diameter, 2 cm in length, and with a surface magnetic intensity of approximately 306 mT) to induce magnetic deformation of the tube (inset of Fig. 3d). We found that when the thickness *x* of the PDMS tube was larger than 110 μm, it was difficult to deform the actuator. When the thickness *x* of the PDMS tube was smaller than 110 μm, it was relatively easy to deform the actuator even though the width of the magnetic layer *y* was only several micrometers (Fig. 3d). The magnetic response process was reversible. When the magnetic field was removed, the actuator immediately recovered its original shape. In addition, the magnetic polymer layer was stable and did not detach from the PDMS tube substrate. The magnetic layer exhibited no obvious change even after 2 years of storage at ambient temperature and after 800 cycles of alternating deformation and recovery processes (Fig. S8).

Magnetic superhydrophobic tubular PDMS that could be deformed under a magnetic field was defined as the actuator (M-SPDMS-A) and was utilized for investigations of directional water transport. The M-SPDMS-A with the magnetic coating side facing up was fixed on a piece of relatively hard paper (ca. 0.22 mm in thickness), and then a water droplet (ca. 10 μL) was added to the actuator. As shown on the left side of Fig. 4a, an external magnetic field was applied to control transport of the water droplet. With a predefined motion of the magnet from left to right, the M-SPDMS-A deformed correspondingly and interacted with the water droplet. As the inner surface of the actuator was superhydrophobic, the adhesive interaction between the water droplet and the inner surface of the actuator was weak and resulted in water droplet transport along the moving direction of the magnet. When the moving direction of the magnet was reversed from right to left, the water droplet was also propelled to move in the reverse direction. The experimental results are shown to the right of Fig. 4a (Movie S2). No obvious water residue was left on the inner surface during the transport process. The transport velocity of the water droplet could be tailored by changing the moving speed of the cylinder magnet. As shown in Fig. 4b–e, we demonstrated that the transport velocity of the water droplet was well controlled. The highest speed was

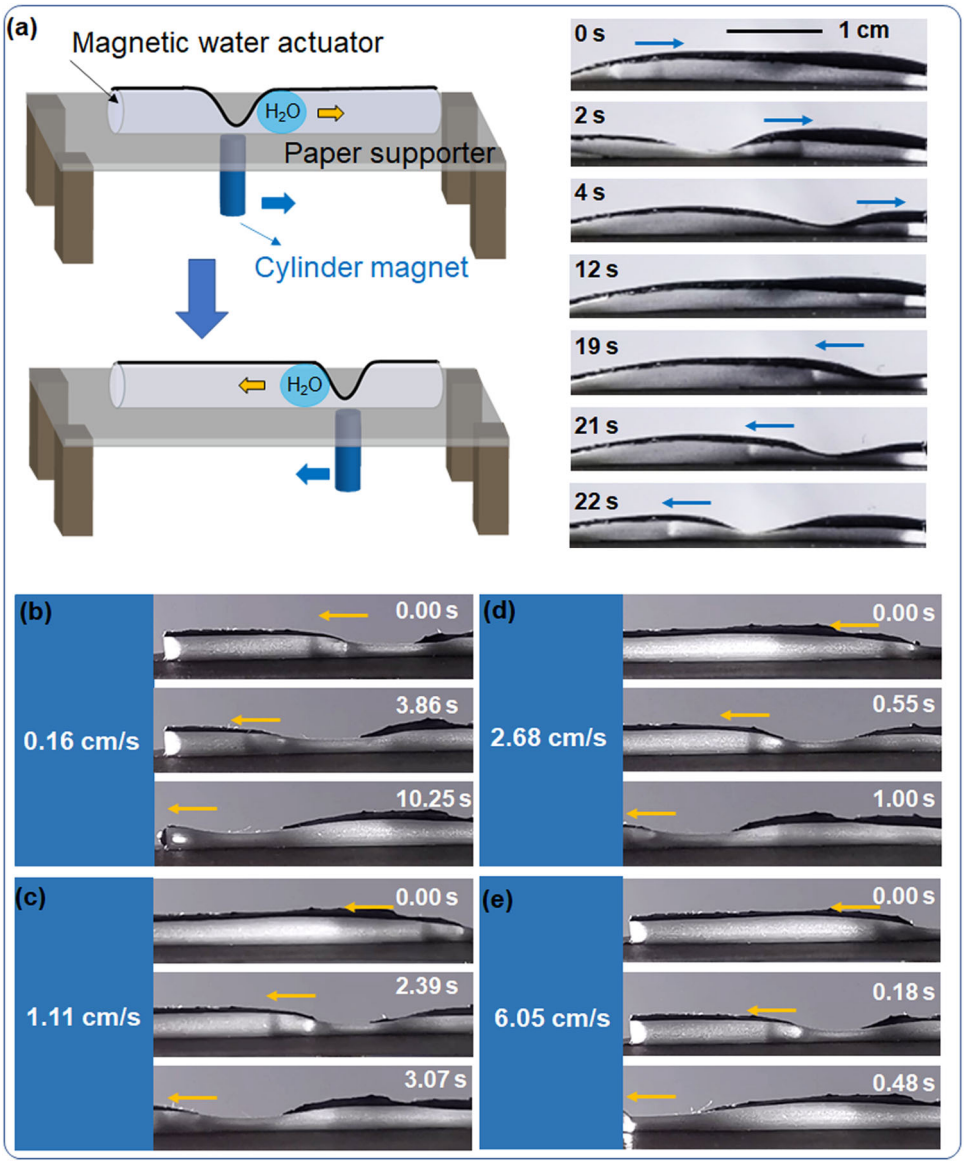

Fig. 4 Magnetic control of water transport in the M-SPDMS-A. a A water droplet is directionally propelled by an applied magnetic field from left to right and in the reverse direction. The left panel is a schematic illustration of the magnetic water transport, and the right is the experimental demonstration (Movie S2). Magnetic control of water transport with different velocities: **b** 0.16 cm/s, **c** 1.11 cm/s, **d** 2.68 cm/s and **e** 6.05 cm/s (Movie S3).

~6.05 cm/s (Movie S3). The driving force (F_d) was mainly attributed to the Laplace pressure gradient arising from the ends of the droplets when the magnetic field was applied to mechanically deform the actuator and the droplet (Fig. S9)[47]. The resistance forces included viscous resistance (F_v) and an adhesive force (F_a) resulting from contact angle hysteresis. Both F_v and F_a were small, and the water droplet was easily propelled by the Laplace pressure gradient. However, when the magnet was moved too fast, the actuator and water droplet were not able to deform quickly enough, and the water droplet failed to move. For a more detailed analysis, refer to S-1 in the Supporting Information. When we utilized a magnet with a stronger magnetic field intensity (~474 mT), the actuator could be deformed quickly, and the water transport velocity was increased up to ~16.1 cm/s (Fig. S10), which is the highest velocity measured for water transport in a closed actuator system (Table S1). We also successfully achieved magnetic transport of liquids widely used in biomedical engineering with the S-PDMS-A, such as phosphate buffer solution (PBS, 0.1 M, pH 7.4), artificial urine (pH 4.5) and sweat (pH 5.5) (Fig. S11).

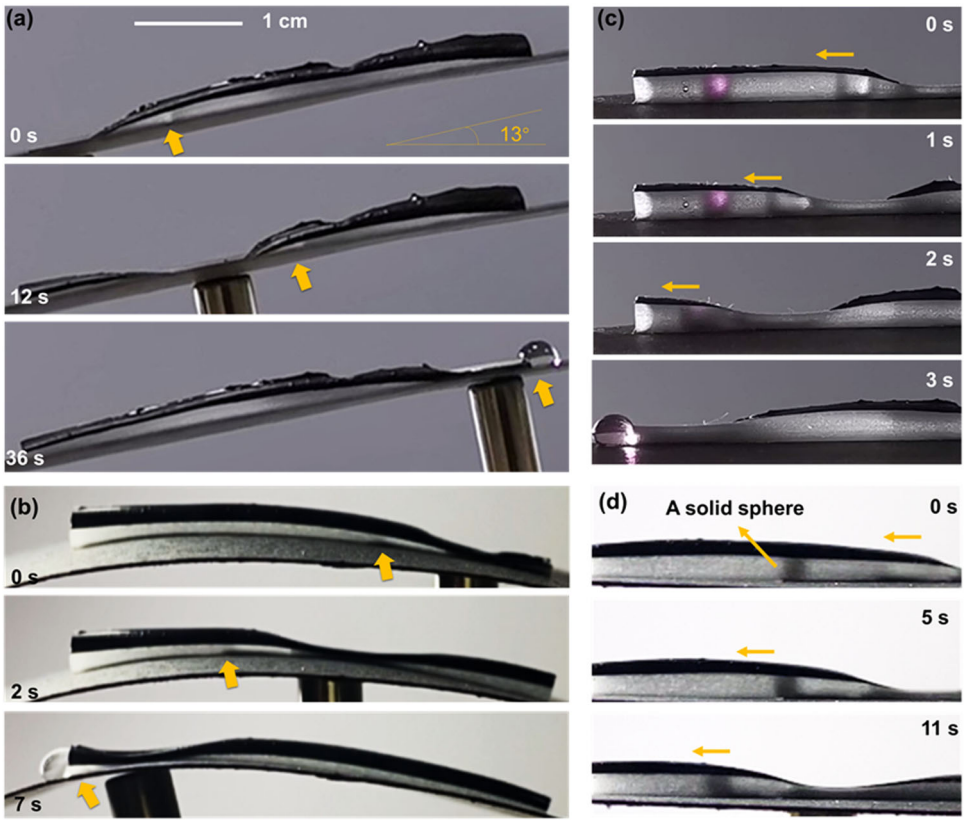

Fig. 5 Magnetic manipulation of water droplets with different functions. a Water droplet transport along a slope under the control of a magnetic field. **b** Water droplet moves on an arch-shaped substrate in the M-SPDMS-A under the control of a magnetic field. **c** Water droplet moves from the right to the left and coalesces with another droplet in the M-SPDMS-A under the control of a magnetic field. **d** Water droplet carries and conveys a solid polymer sphere, which is indicated by an arrow in the image.

The water droplet inside the actuator could be propelled to move along a slope. Without an externally applied magnetic field, the water droplet inside the actuator moved downward due to gravity when the tilt angle β was larger than 6° (Fig. S12). A larger tilt angle led to a larger driving force and higher water transport speed in a relatively shorter time (Fig. S12b–e). With manipulation of the applied magnetic field, the water droplet was propelled uphill on a slope with a 13° incline (Fig. 5a) and move on an arch-shaped substrate (Fig. 5b). In addition, water droplets could also be driven to coalesce with another droplet inside the actuator or capture and convey small solid guests. As shown Fig. 5c, a rhodamine B (RhB)-loaded water droplet was located inside the left part of the actuator, and another water droplet was manipulated by the magnetic field to move toward the dyed droplet and finally coalesced. Similarly, capture and conveyance of a millimeter resin sphere by a water droplet was achieved, as shown in Fig. 5d. These experiments showed the potential of the magnetic actuator for applications involving controlled reactions and guest delivery.

Superhydrophobic surfaces are known to have weak interactions with water droplets because of the smaller contact area between the droplet and the structured surface. This unique property has been utilized to transport water solutions and biological samples with negligible loss of liquid weight[44,48,49]. Here, water loss in the transport process was also investigated. To conveniently observe liquid loss, water droplets containing RhB (10^{-6} M) were used for the study. As shown in Fig. 6a, after addition into the M-SPDMS-A, the water droplet was propelled by the magnetic field and transported toward the left open side and easily moved out. In contrast, a magnetic PDMS tube without microstructures on the inner surface was prepared and used to actuate the water droplet (Fig. 6b). The droplet adhered to the inner surface due to the strong contact adhesion and could not be driven out. These results further indicated the importance of the micro/nanostructures in the M-SPDMS-A. Then, both inner surfaces the droplet contacted were investigated with laser fluorescence confocal microscopy. Some microscale areas of the M-SPDMS-A exhibited red fluorescence (Fig. 6c); this was due to the

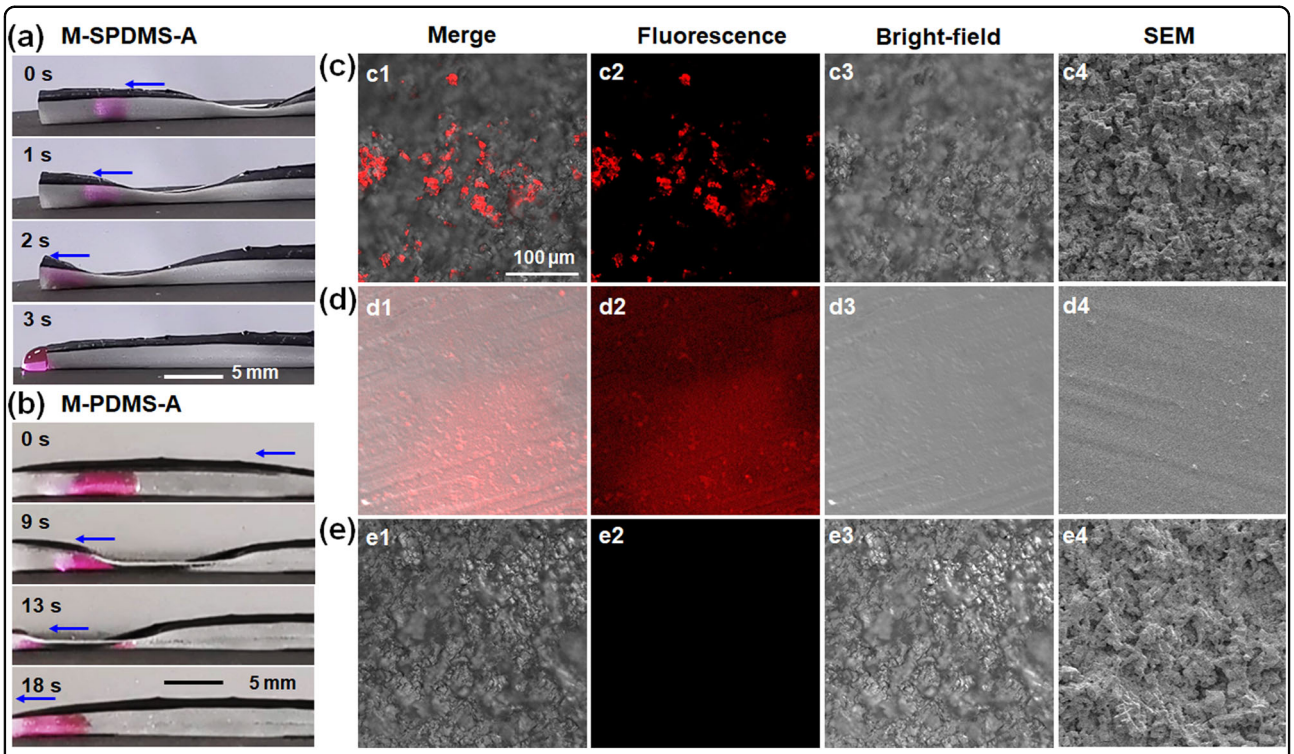

Fig. 6 Liquid loss test of magnetic liquid actuators forwater droplet transport. Magnetic transport of water droplets in the M-SPDMS-A (**a**) and M-PDMS-A (**b**). RhB (10-6 M) was added into the droplets for convenient characterization. Laser scanning confocal microscopy and SEM images of the inner surfaces of M-SPDMS-A from (**a**), M-PDMS-A from (**b**) and a controlled superhydrophobic PDMS is shown in (**c**), (**d**) and (**e**), respectively.

presence of RhB, as pure PDMS has no fluorescence (Fig. 6e). For the sample from Fig. 6b, the whole area was found to exhibit red fluorescence, which resulted from the large contact area between the water droplet and the PDMS surface (Fig. 6d). SEM indicated that there was no obvious change for any sample. The comparison clearly showed that the M-SPDMS-A allowed only negligible water loss during the transport process, which is important in some practical applications, e.g., in transporting valuable samples. We further investigated magnetic transport of PBS (0.1 M, pH 7.4), artificial urine (pH 4.5), and artificial sweat (pH 5.5) by the M-SPDMS-A and determined the liquid loss. RhB was also added to the liquids for residue detection. All experiments indicated negligible liquid loss by M-SPDMS-A compared with the control (Fig. S13).

Conclusion

To summarize, we demonstrated a new magnetic PDMS tubular actuator. Its inner surface was superhydrophobic and had weak interactions with water droplets. Under an applied magnetic field, the water droplet could be efficiently controlled to move with different velocities. The highest velocity was 16.1 cm/s. In addition, due to the superhydrophobic properties of the inner surface, the contact area between the water droplet and the PDMS inner surface was small, and the liquid loss was negligible. This work provides a new strategy for manipulating liquids rapidly and with minimal loss, which indicates promise for use in drug delivery, droplet-based analyses, and water collection.

Acknowledgements

This work is supported by the National Natural Science Foundation of China (22090050, 21874121), the National Key R&D Program of China (2021YFA1200403, 2018YFE0206900), the Joint NSFC-ISF Research Grant Program (Grant No: 22161142020), the Natural Science Foundation of Hubei Province (2020CFA037), Zhejiang Provincial Natural Science Foundation of China under Grant No. LD21B050001.

Author details

[1]Faculty of Materials Science and Chemistry, China University of Geosciences, Wuhan 430074, People's Republic of China. [2]State Key Laboratory of Biogeology and Environmental Geology, China University of Geosciences, Wuhan 430074, People's Republic of China. [3]Engineering Research Center of Nano-Geomaterials of Ministry of Education, China University of Geosciences, Wuhan 430074, People's Republic of China

Author contributions

L.C. and F.X. conceived and designed the overall experiments. F. (Y)X., L.Z., L.X., J.L., C.J., and L.C. performed the experiments and collected the data. L.Z. performed the supplementary experiments. F. (Y) X., and L.C. wrote the paper. L.C. and F.X. revised the paper. All authors reviewed the manuscript.

Competing interests

The authors declare no competing interests.

Supplementary information The online version contains supplementary material available at https://doi.org/10.1038/s41427-022-00431-2.

Received: 30 April 2022 Revised: 13 August 2022 Accepted: 15 August 2022.
Published online: 21 October 2022

References

1. Zheng, Y. et al. Directional water collection on wetted spider silk. *Nature* **463**, 640–643 (2010).
2. Zhang, Q. et al. Highly flexible monolayered porous membrane with superhydrophilicity–hydrophilicity for unidirectional liquid penetration. *ACS Nano* **14**, 7287–7296 (2020).
3. Damak, M. & Varanasi, K. Electrostatically driven fog collection using space charge injection. *Sci. Adv.* **4**, eaao5323 (2018).
4. Joanicot, M. & Ajdari, A. Droplet control for microfluidics. *Science* **309**, 887–888 (2005).
5. Whitesides, G. M. The origins and the future of microfluidics. *Nature* **442**, 368–373 (2006).
6. Zhu, P. & Wang, L. Microfluidics-enabled soft manufacture of materials with tailorable wettability. *Chem. Rev.* **122**, 7010–7060 (2022).
7. Daniel, S., Chaudhury, M. K. & Chen, J. C. Fast drop movements resulting from the phase change on a gradient surface. *Science* **291**, 633–636 (2001).
8. Tang, Y., Yang, X., Li, Y., Lu, Y. & Zhu, D. Robust micro-nanostructured superhydrophobic surfaces for long-term dropwise condensation. *Nano Lett.* **21**, 9824–9833 (2021).
9. Hou, Y. et al. Tunable water harvesting surfaces consisting of biphilic nanoscale topography. *ACS Nano* **12**, 11022–11030 (2018).
10. Wisdom, K. M. et al. Self-cleaning of superhydrophobic surfaces by self-propelled jumping condensate. *Proc. Natl Acad. Sci. USA* **110**, 7992–7997 (2013).
11. Su, M. & Song, Y. Printable smart materials and devices: Strategies and applications. *Chem. Rev.* **122**, 5144–5164 (2022).
12. Wu, L. et al. Bioinspired ultra-low adhesive energy interface for continuous 3D printing: Reducing curing induced adhesion. *Research* **2018**, 4795604 (2018).
13. Feng, W., Ueda, E. & Levkin, P. A. Droplet microarrays: From surface patterning to high-throughput applications. *Adv. Mater.* **30**, 1706111 (2018).
14. Li, H. et al. Droplet precise self-splitting on patterned adhesive surfaces for simultaneous multidetection. *Angew. Chem. Int. Ed.* **59**, 10535–10539 (2020).
15. Cira, N. J., Benusiglio, A. & Prakash, M. Vapour-mediated sensing and motility in two-component droplets. *Nature* **519**, 446–450 (2015).
16. Li, K. et al. Structured cone arrays for continuous and effective collection of micron-sized oil droplets from water. *Nat. Commun.* **4**, 2276 (2013).
17. Feng, S. et al. Three-dimensional capillary ratchet-induced liquid directional steering. *Science* **373**, 1344–1348 (2021).
18. Li, F., Wang, Z., Huang, S., Pan, Y. & Zhao, X. Flexible, durable, and unconditioned superoleophobic/superhydrophilic surfaces for controllable transport and oil–water separation. *Adv. Funct. Mater.* **28**, 1706867 (2018).
19. Nge, P. N., Rogers, C. I. & Woolley, A. T. Advances in microfluidic materials, functions, integration, and applications. *Chem. Rev.* **113**, 2550–2583 (2013).
20. Li, A. et al. Programmable droplet manipulation by a magnetic-actuated robot. *Sci. Adv.* **6**, eaay5808 (2020).
21. Parker, A. R. & Lawrence, C. R. Water capture by a desert beetle. *Nature* **414**, 33–34 (2001).
22. Prakash, M., Quéré, D. & Bush, J. W. M. Surface tension transport of prey by feeding shorebirds: The capillary ratchet. *Science* **320**, 931–934 (2008).
23. Ju, J. et al. A multi-structural and multi-functional integrated fog collection system in cactus. *Nat. Commun.* **3**, 1247 (2012).
24. Soltani, M. & Golovin, K. Lossless, passive transportation of low surface tension liquids induced by patterned omniphobic liquidlike polymer brushes. *Adv. Funct. Mater.* **32**, 2107465 (2022).
25. Wang, Q. Q., He, Y., Geng, X. X., Hou, Y. P. & Zheng, Y. M. Enhanced fog harvesting through capillary-assisted rapid transport of droplet confined in the given microchannel. *ACS Appl. Mater. Interfaces* **13**, 48292–48300 (2021).
26. Meng, Q. A. et al. Controlling directional liquid transport on dual cylindrical fibers with oriented open-wedges. *Adv. Mater. Interfaces* **9**, 2101749 (2022).
27. Geng, H. et al. Sunlight-driven water transport via a reconfigurable pump. *Angew. Chem. Int. Ed.* **57**, 15435–15440 (2018).
28. Dai, H., Dong, Z. & Jiang, L. Directional liquid dynamics of interfaces with superwettability. *Sci. Adv.* **6**, eabb5528 (2020).
29. Sun, Q. et al. Surface charge printing for programmed droplet transport. *Nat. Mater.* **18**, 936–941 (2019).
30. Li, C. et al. Bioinspired inner microstructured tube controlled capillary rise. *Proc. Natl Acad. Sci. USA* **116**, 12704–12709 (2019).
31. Chen, H. et al. Continuous directional water transport on the peristome surface of Nepenthes alata. *Nature* **532**, 85–89 (2016).
32. Lei, W. et al. High-speed transport of liquid droplets in magnetic tubular microactuators. *Sci. Adv.* **4**, eaau8767 (2018).
33. Dorvee, J. R., Derfus, A. M., Bhatia, S. N. & Sailor, M. J. Manipulation of liquid droplets using amphiphilic, magnetic one-dimensional photonic crystal chaperones. *Nat. Mater.* **3**, 896–899 (2004).
34. Pollack, M. G., Fair, R. B. & Shenderov, A. D. Electrowetting-based actuation of liquid droplets for microfluidic applications. *Appl. Phys. Lett.* **77**, 1725–1726 (2000).
35. Dai, H. et al. Controllable high-speed electrostatic manipulation of water droplets on a superhydrophobic surface. *Adv. Mater.* **31**, 1905449 (2019).
36. Brzoska, J. B., Brochard-Wyart, F. & Rondelez, F. Motions of droplets on hydrophobic model surfaces induced by thermal gradients. *Langmuir* **9**, 2220–2224 (1993).
37. Linke, H. et al. Self-propelled Leidenfrost droplets. *Phys. Rev. Lett.* **96**, 154502 (2006).
38. Lagubeau, G., Le Merrer, M., Clanet, C. & Quéré, D. Leidenfrost on a ratchet. *Nat. Phys.* **7**, 395–398 (2011).
39. Chen, G. et al. Magnetically responsive film decorated with microcilia for robust and controllable manipulation of droplets. *ACS Appl. Mater. Interfaces* **13**, 1754–1765 (2021).
40. Zhao, Y., Fang, J., Wang, H., Wang, X. & Lin, T. Magnetic liquid marbles: manipulation of liquid droplets using highly hydrophobic Fe_3O_4 nanoparticles. *Adv. Mater.* **22**, 707–710 (2010).
41. Tian, D. et al. Fast responsive and controllable liquid transport on a magnetic fluid/nanoarray composite interface. *ACS Nano* **10**, 6220–6226 (2016).
42. Xu, B., Zhu, C. Y., Qin, L., Wei, J. & Yu, Y. L. Light-directed liquid manipulation in flexible bilayer microtubes. *Small* **15**, e1901847 (2019).
43. Lv, J. A. et al. Photocontrol of fluid slugs in liquid crystal polymer microactuators. *Nature* **537**, 179–184 (2016).
44. Kim, S., Cho, H. & Hwang, W. Simple fabrication method of flexible and translucent high-aspect ratio superhydrophobic polymer tube using a repeatable replication and nondestructive detachment process. *Chem. Eng. J.* **361**, 975–981 (2019).
45. Tian, Y., Su, B. & Jiang, L. Interfacial material system exhibiting superwettability. *Adv. Mater.* **26**, 6872–6897 (2014).
46. Chu, Z. & Seeger, S. Superamphiphobic surfaces. *Chem. Soc. Rev.* **43**, 2784–2798 (2014).
47. Stamatopoulos, C. et al. Droplet self-propulsion on superhydrophobic microtracks. *ACS Nano* **14**, 12895–12904 (2020).
48. Wang, J. et al. Preparation of superhydrophobic flexible tubes with water and blood repellency based on template method. *Colloids Surf. A* **587**, 124331 (2020).
49. Nokes, J. M. et al. Reduced blood coagulation on roll-to-roll, shrink-induced superhydrophobic plastics. *Adv. Healthc. Mater.* **5**, 593–601 (2016).